# INSIDE-OUT CONFIGURATION ACTIVE MAGNETIC BEARING ACTUATORS

M.A. Pichot, J.P. Kajs, R.J. Hayes, J.H. Beno, A. Ouroua, and B.M. Rech

University of Texas at Austin
Center for Electromechanics

## ABSTRACT

The University of Texas Center for Electromechanics (UT-CEM) has designed active magnetic bearing actuators for use in a 5 MW flywheel alternator with a 700 lb (318 kg), 20,000 rpm rotor, under the sponsorship of the Department of Defense Combat Hybrid Power Systems (CHPS) program. Because this machine incorporates an unusual inside-out topology (i.e., the rotating portion of the flywheel is located outside the stationary components), unique inside-out configuration magnetic bearing actuators are required. Permanent magnet bias bearings were chosen for this application because of inherent low power requirements, low power losses, and nearly linear current stiffness and positional stiffness. To verify performance, a bearing test fixture was designed and built which permits static and dynamic force measurement. This paper discusses bearing requirements, actuator design, predicted performance, and compares theoretical versus measured bearing characteristics. A companion paper discusses control issues for this unique magnetic bearing system [1].

## INTRODUCTION

The CHPS program seeks to produce a new class of hybrid-electric combat vehicles with significant advances in the areas of mobility, armaments, and defensive systems. One of the distinguishing features of these vehicles is that all major subsystems will be electrically driven, including a hybrid electric drive-train system, electric armaments and electromagnetic armor. An illustration for the vehicle concept appears in figure 1.

UT-CEM serves as a subcontractor in this project, with the task of developing a flywheel alternator to deliver pulsed power for weapons systems as well as load-leveling power for drive-train components. High power electrical loads for the alternator include the following weapons systems: an electrothermal-chemical (ETC) gun, high power lasers, and electromagnetic armor. The alternator also provides power for AC induction traction motors used for propulsion and for a fully active electromagnetic suspension system.

Since the flywheel alternator will be mounted onboard the vehicle, its weight and volume are of prime importance. Accordingly, the alternator is designed to maximize energy density and operate at high speed. Energy storage for this machine is 25 MJ at 20,000 rpm with an estimated alternator weight of 1,310 lb (595 kg). It provides up to 5 MW peak power for intermittent weapon systems loads and 350 kW continuous power for propulsion related loads.

This work was supported by the U.S. Defense Advanced Research Projects Agency under letter subcontract #4500152859.

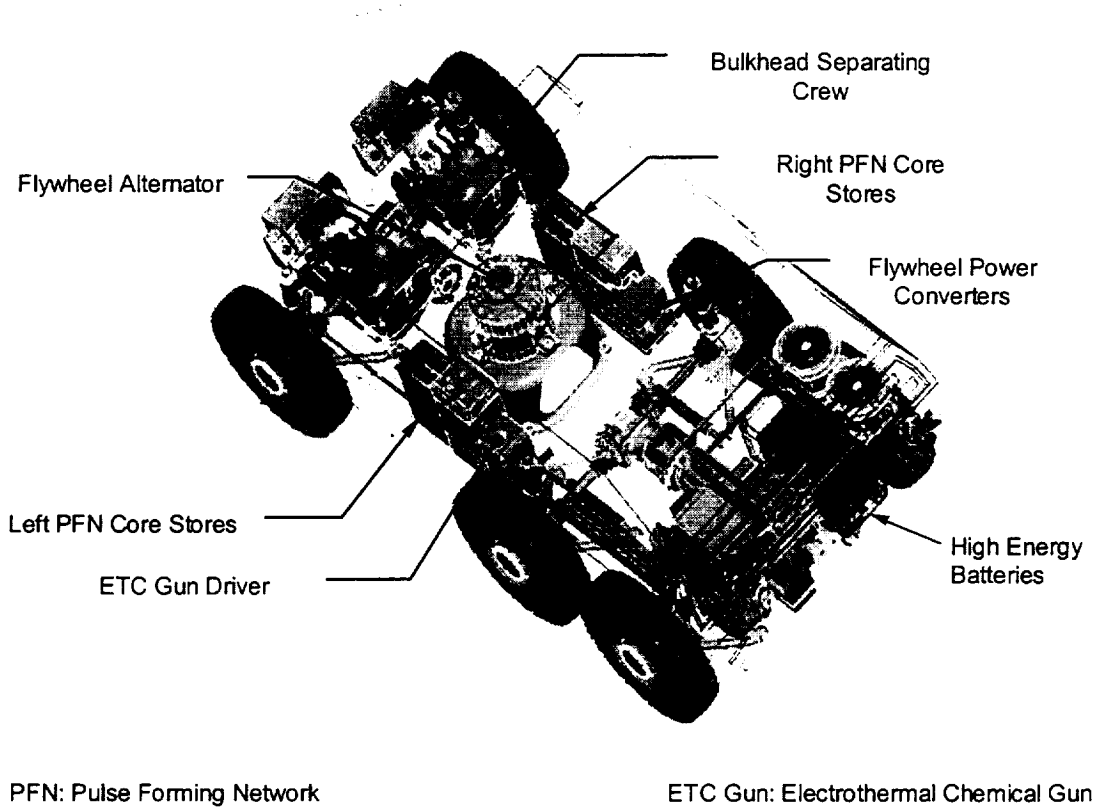


*Figure 1. CHPS hybrid electric combat vehicle.*

A cross-sectional view of the CHPS flywheel alternator is shown in figure 2 (note that the alternator is a vertical axis machine in the vehicle). The inside-out topology shown is very efficient in terms of maximizing energy stored per unit volume, but creates challenging bearing requirements. Rolling element bearings were first investigated for use in the CHPS machine, but proved unattractive for several reasons including: excessive rolling element bearing power loss and heat generation for this continuous duty machine, difficult lubrication and cooling because the rotor spins in a vacuum, and inadequate calculated bearing life.

For these reasons, a magnetic bearing system was selected over rolling element bearings, despite increased complexity. Since magnetic bearings are the only bearing type that appears compatible with the CHPS flywheel requirements, development of inside-out bearing actuators is viewed as essential to successful flywheel design.

## BEARING SYSTEM REQUIREMENTS

The bearing system for the flywheel alternator must have sufficient capabilities to deal with rotor static and dynamic loads common to all high-speed machines. In addition, since mounted in a combat vehicle with off-road capabilities, terrain loads are transmitted through the vehicle suspension and will be present at the bearings. To reduce windage power losses, the alternator

rotor operates in a vacuum, necessitating a vacuum-compatible bearing system. Cooling oil is available in the stator shaft at 70-90°C. A summary of the magnetic bearing system requirements appears in table 1.

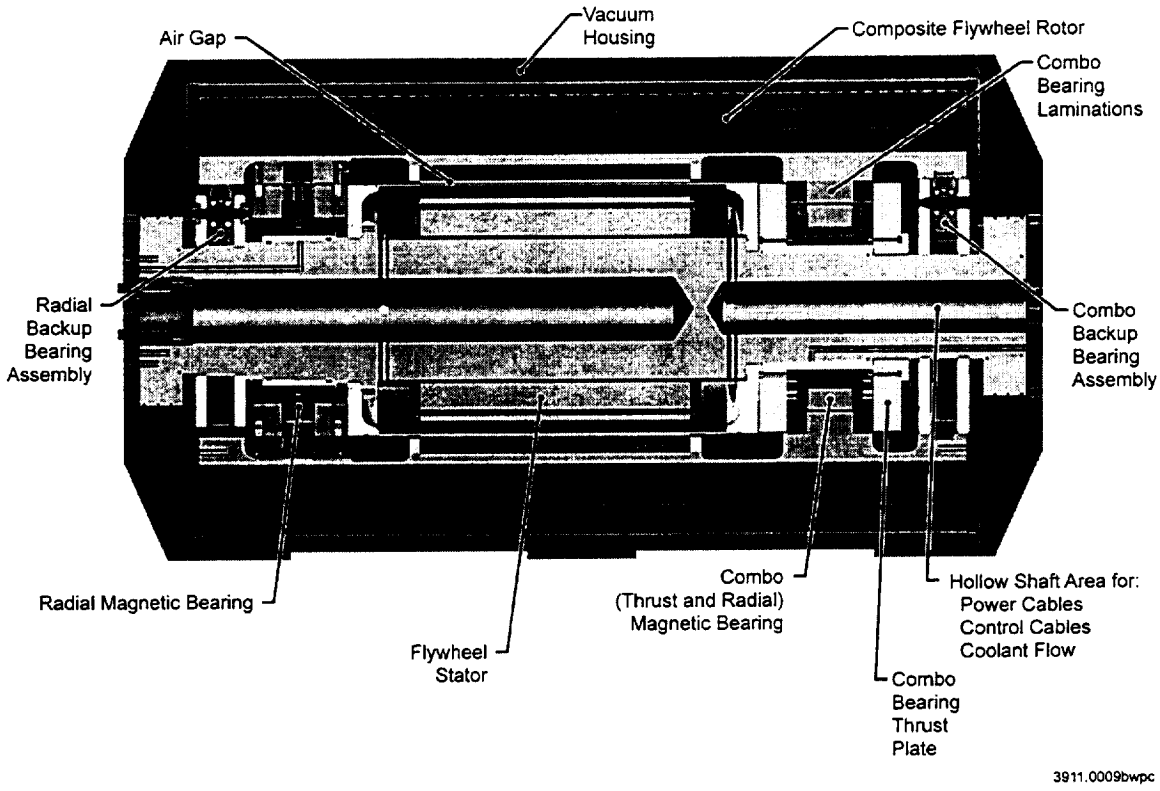


*Figure 2. CHPS flywheel alternator.*

*Table 1. Magnetic Bearing System Requirements*

| | |
|---|---|
| Maximum Speed | 20,000 rpm |
| Normal Operating Speed Range | 15,000 – 20,000 rpm |
| Load Capacity | 2g dynamic load capacity (plus 1g static load) |
| Maximum Power Loss | ~100 W per bearing |
| Frequency Response<br>Radial Actuators<br><br>Thrust Actuator | <br>Bandwidth at least 10X machine rotational frequency [1]<br>Full load capacity at 2X machine rotational frequency<br>Bandwidth of approximately 10 Hz desired |
| Backup Bearing Requirements | Provide support when magnetic bearings not levitated<br>Shut down from full speed with magnetic bearing system inactive<br>Provide support for short duration loads exceeding magnetic bearing load capacity (up to 8g maximum) |

## BEARING SYSTEM DESIGN

### Magnetic Bearing Type

Permanent magnet bias homopolar (PMBH) magnetic bearings were selected for this application based on studies showing reduced power requirements and lower losses compared to heteropolar bearings [2]. An additional benefit of PMBH bearings is that control is simplified because of nearly linear current stiffness and positional stiffness characteristics.

Although PMBH bearings have been described in the literature previously [3], the CHPS machine presents an unusual application due to its inside-out topology. Since the rotational portion of the bearings is positioned outboard of the stator at a relatively large radius, bearing rotor laminations must withstand higher stresses than in conventional magnetic bearings. In addition, the magnetic air gap grows larger with increasing speed, instead of decreasing as in conventional configuration bearings. These factors complicate the bearing actuator design, and for our application, necessitate the use of unconventional bearing materials.

### Bearing System Configuration

As shown in figure 2, the bearing configuration chosen consists of a radial magnetic bearing used on one end of the rotor and a combination bearing on the other. The radial bearing provides support in the radial direction only, while the combination bearing supports loads in both radial and axial directions. The advantage of this arrangement is that the combination bearing is significantly shorter in the axial direction than separate radial and thrust bearings, and allows the CHPS machine to be more compact than if separate bearings were used.

Also incorporated in the magnetic bearing system are backup bearings. These bearings provide support during nonoperational periods when the magnetic bearings are inactive, and provide a means to shut down the machine safely in the event of a magnetic bearing system failure. In addition, in the CHPS machine the backup bearings must occasionally provide additional support for short duration loads exceeding the magnetic bearing load capacity. Infrequent loads as high as $8g$ can be expected on combat vehicles from terrain shock loads transmitted through the vehicle suspension. It would be prohibitive to use bearing actuators with enough capacity to handle these loads (the bearings would be too large to be practical), so the backup bearings are required to accept these additional loads.

### Bearing Design Process

The bearing design for this application is approached with an iterative process involving consideration of several system components, and takes the following form:

- Develop a model of the entire system to determine requirements (includes control and rotor dynamics modeling)
- Design baseline actuators (using design codes discussed later in this paper)

- Analyze system model including actuators, amplifiers, sensor dynamics, and control algorithms
- Iterate system design until an acceptable design is identified

## RADIAL BEARING ACTUATOR DESIGN

An illustration of the radial bearing actuator is shown in figure 3. The inside-out configuration is readily apparent in the fact that the outer part of the bearing includes the rotor lamination assembly, with the inner part of the bearing consisting of stator components. The radial bearing is 14.17 in. (36.0 cm) on the outside diameter with an overall length of 4.33 in. (11.0 cm), and a radial air gap 0.020 in. (0.051 cm) at rest. At 20,000 rpm, the radial air gap increases to 0.049 in. (0.125 cm).

In this bearing design, the bias field is established with neodymium-iron-boron (NdFeB) permanent magnets located in the center of the stator. The magnets are segmented and sandwiched between two solid stator iron components manufactured from low carbon steel. Stator laminations are fabricated from 0.014 in. (0.356 mm) thick M-19 silicon steel and include dovetail-shaped coil slots to reduce rotor lamination rotating losses. The stator laminations are assembled to the stator iron with an interference fit to provide high rigidity in the radial direction and for good mechanical integrity. A hydraulic fit is used for bearing stator assembly to the alternator shaft, providing an interference fit for high radial rigidity, but in a form that can be repeatedly reassembled. Each of the eight actuator coils is wound with 90 turns of No. 19 polyester coated copper magnet wire, with G-10 coil guides provided to simplify the winding process.

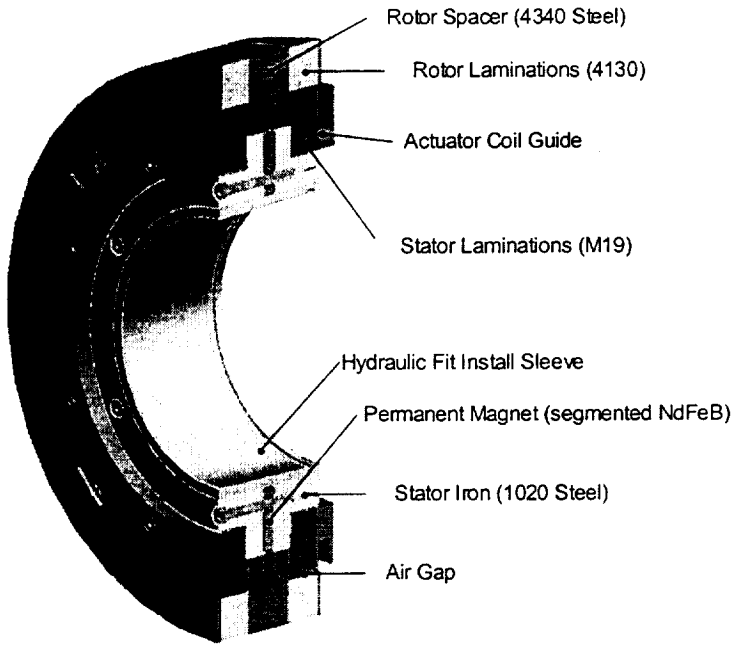


*Figure 3. Radial bearing actuator.*

From an electromagnetic point of view, silicon steel would also be a good choice for the rotor laminations; however, silicon steel does not have adequate mechanical properties to withstand induced rotor stresses and corresponding fatigue conditions. A structural grade steel (AISI 4130) was ultimately chosen for the rotor laminations for desirable strength and fatigue characteristics, despite less desirable electromagnetic properties.

## COMBINATION BEARING ACTUATOR DESIGN

The CHPS combination bearing actuator is shown in figure 4. As with the radial bearing, the outer part of the bearing rotates with the flywheel rotor, with the stator bearing components assembled to the flywheel stator shaft. The combination bearing is 12.0 in. (30.5 cm) outside diameter with an overall length of 6.58 in. (16.7 cm), and radial and thrust air gaps 0.020 in. (0.051 cm) at rest. At 20,000 rpm, the radial air gap increases to 0.036 in. (0.091 cm). As discussed earlier, this bearing provides support in both radial and axial directions, eliminating the need for separate radial and thrust bearings. This is accomplished with separate actuator coils for the radial and axial directions, which generate forces in separate radial and thrust air gaps. As with the radial bearing, bias flux is provided with NdFeB permanent magnets, although in the combination bearing, the magnets are magnetized in the radial instead of the axial direction. The combination bearing also employs a hydraulic fit install sleeve and includes segmented wedges as shown; these devices permit assembly and disassembly into the CHPS flywheel topology.

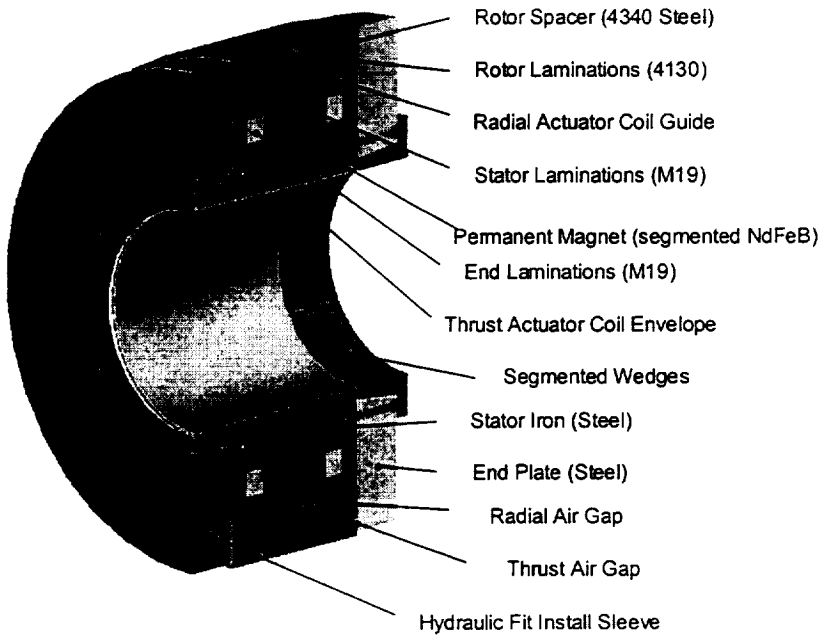


*Figure 4. Combination bearing actuator.*

Materials chosen for the combination bearing are similar to the radial bearing, with rotor laminations made from AISI 4130 steel, stator iron and end plate components made from low-carbon steel, and stator laminations fabricated from M-19 silicon steel. The combination bearing requires four radial actuator coils of 75 turns each, wound with No. 20 copper magnet wire. Two thrust actuator coils are required, each consisting of 190 turns of No. 20 magnet wire.

## ACTUATOR ANALYSIS AND PREDICTED PERFORMANCE

A variety of analyses were performed in the design of the CHPS magnetic bearing actuators, including modeling of actuator electromagnetics, thermal response, mechanical stress and fatigue, and control system behavior. This paper will present results from the electromagnetic analysis, with control system modeling discussed in a companion paper [1].

For actuator electromagnetic analysis, a 1-D non-linear magnetic circuit code for inside-out actuators was developed at UT-CEM. It includes modeling of non-linear B-H characteristics and calculations necessary for sizing of coil conductors to meet required criteria of resistance, voltage, and current. Simplified thermal calculations are also provided for power loss and corresponding temperature rise estimates. Calculation turn-around time is fast, allowing the user to rapidly evaluate candidate bearing geometries during preliminary design optimization.

As a final check in the electromagnetic analysis, 3-D non-linear finite element analysis (FEA) is performed using *Opera-3D* software commercially available from Vector Fields Inc. Figure 5 shows example FEA meshes used for the radial and combination bearings. As shown in the figure, symmetry is used where appropriate to reduce computation time, and actuator coil geometry is accurately modeled.

Predicted bearing force versus DC current is shown in Figure 6 for the radial and combination bearings operating at 20,000 rpm. In-line and diagonal radial force curves are provided, where in-line forces are defined as being in the direction of the bearing poles, and diagonal forces in the direction of the coil slots (at 45° with respect to bearing poles).

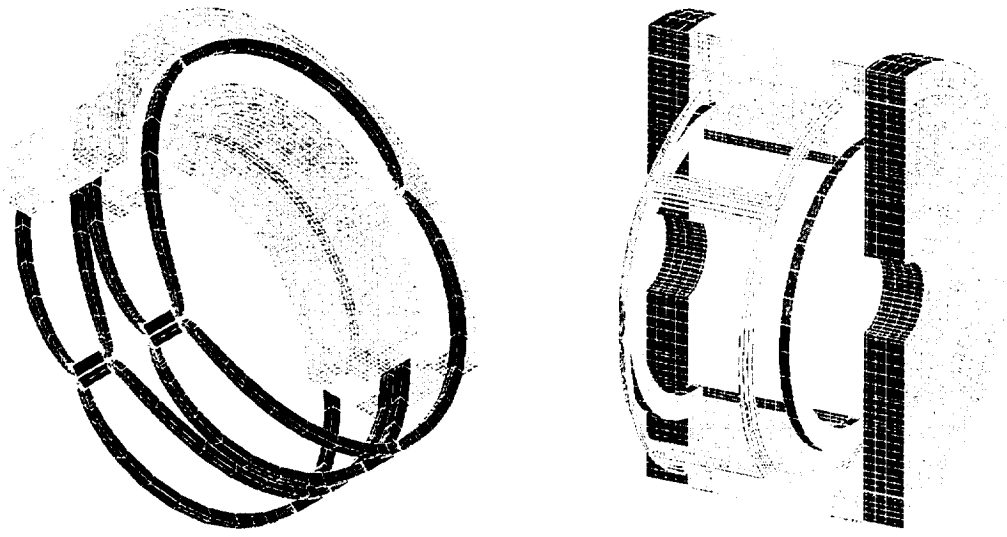

*Figure 5. Radial and combination bearing FEA meshes.*

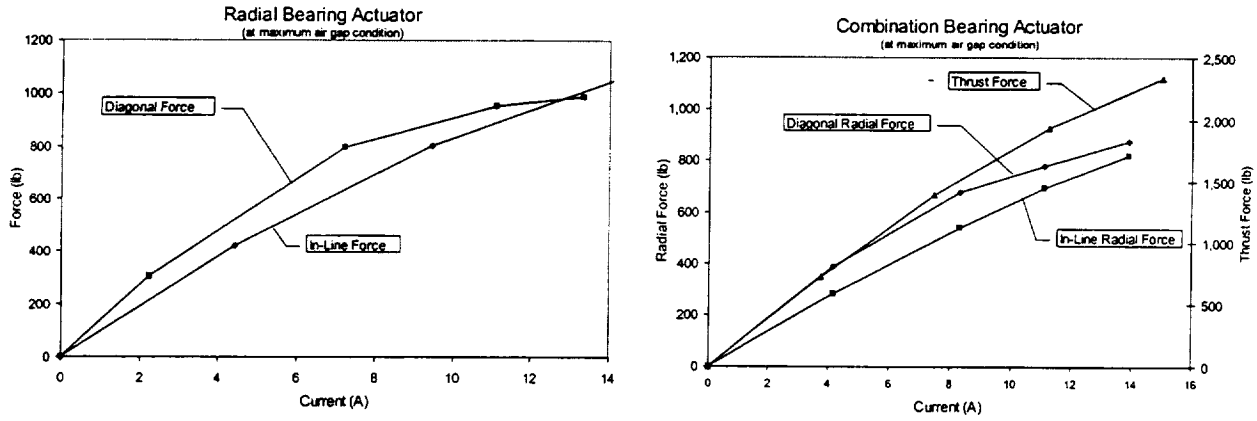


*Figure 6. Predicted actuator force vs. DC current.*

To simplify control, the actuators were designed to meet stated load capacity goals while operating on the linear part of the force versus current curve. Assuming equal distribution of the $2_g$ dynamic load, this corresponds to a required radial force of 700 lb (3.11kN) per bearing. The thrust bearing requires sufficient capacity to support $2_g$ dynamic plus $1_g$ static load for this vertical axis machine, corresponding to 2,100 lb (9.34 kN).

## BEARING TEST HARDWARE

To verify design and analysis codes, and provide first-hand experience with fabrication and operation of the inside-out bearing actuators, UT-CEM fabricated and assembled a radial bearing actuator for testing. To measure bearing characteristics, a non-rotational test fixture was designed and built which permits direct measurement of output force, displacement, coil temperature, and air gap flux density levels. The completed radial test bearing stator appears in figure 7.

An illustration of the radial bearing test fixture is shown in figure 8. The fixture includes a stator shaft that mimics the CHPS flywheel alternator shaft, and is equipped with the hydraulic seals and porting required to demonstrate a test hydraulic fit of the radial bearing onto the stator shaft. For measuring bearing output forces, eight strain-gauge type force transducers are provided; for measuring displacements of the bearing rotor with respect to stator, four eddy current type displacement sensors are used. Thin hall sensors were procured that allow direct measurement of magnetic air gap flux densities. The

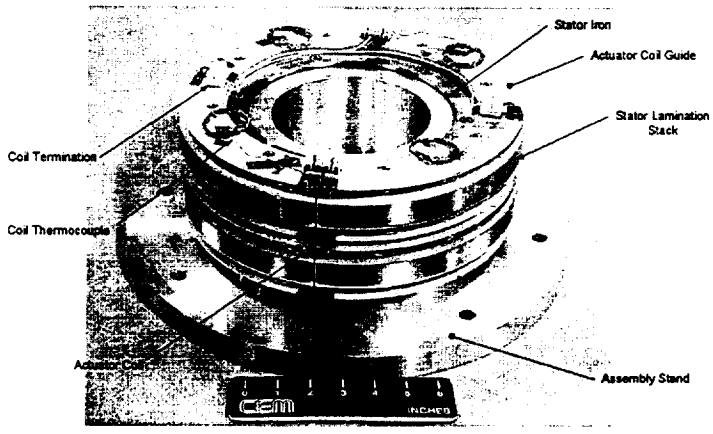


*Figure 7. Radial test bearing stator.*

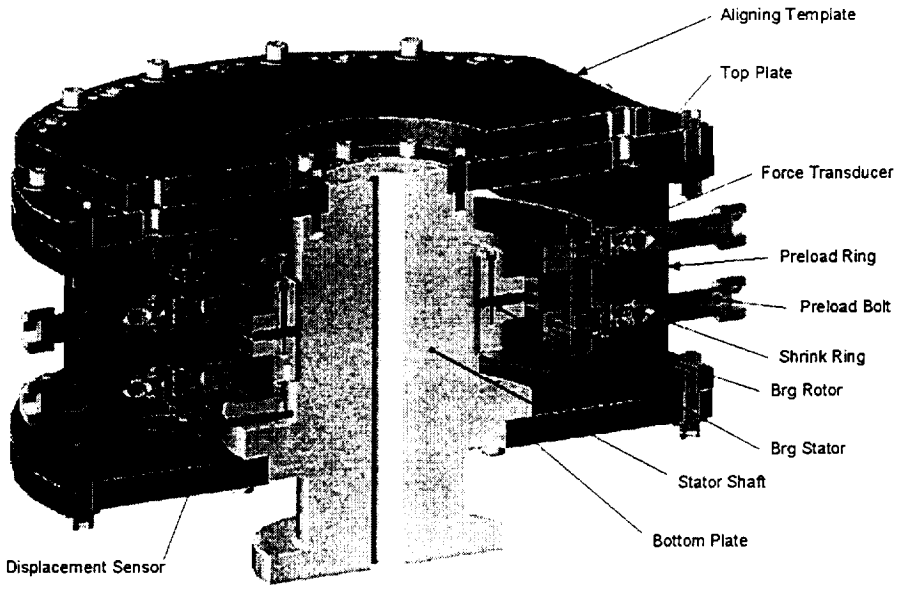


*Figure 8. Radial bearing test fixture.*

test fixture also includes provisions for magnetically centering and making prescribed displacements of the rotor with respect to the stator (useful for positional stiffness measurement).

Data collection and control for the bearing testing was done using PC-based control and data acquisition software. Amplifiers used are pulse width modulated type servo amplifiers (designed to drive brush-type DC motors) with 25 A nominal output current capability. The data acquisition system provides a control panel in which desired values are input, commands are sent out to the bearing amplifiers, and the resulting data from the force, displacement, and magnetic field sensors are digitized, displayed on screen, and if desired, written to a spreadsheet file for subsequent review.

This test setup allows measurement of the following bearing characteristics: actuator positional stiffness, air gap flux density distribution, AC and DC output force vs. input current, current stiffness transfer function, and actuator magnetic hysteresis. Photographs of the experimental setup are shown in figure 9.

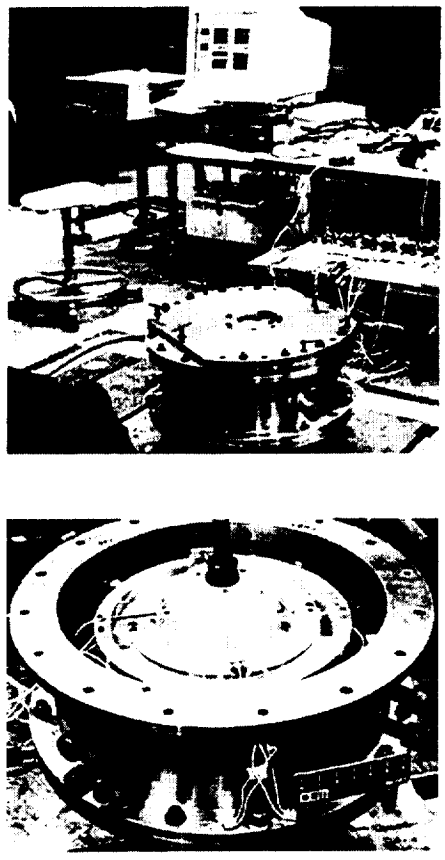

*Figure 9. Bearing test experimental hardware.*

## TEST RESULTS

Before attempting bearing measurements, a test fixture calibration procedure was conducted to ensure accuracy and repeatability. This was done by inserting a small hydraulic cylinder and load cell into the fixture, applying known forces, and establishing a fixture calibration factor, which was thereafter used to adjust force data collected by the data acquisition system. Radial bearing actuator parameters were measured with an air gap corresponding to the zero-speed condition at room temperature. Results are summarized below.

### Impedance Measurement

Measured actuator impedance is shown in figure 10. Predicted DC impedance is 1.4 Ω and 17 mH, which agrees well with the measured zero frequency characteristics.

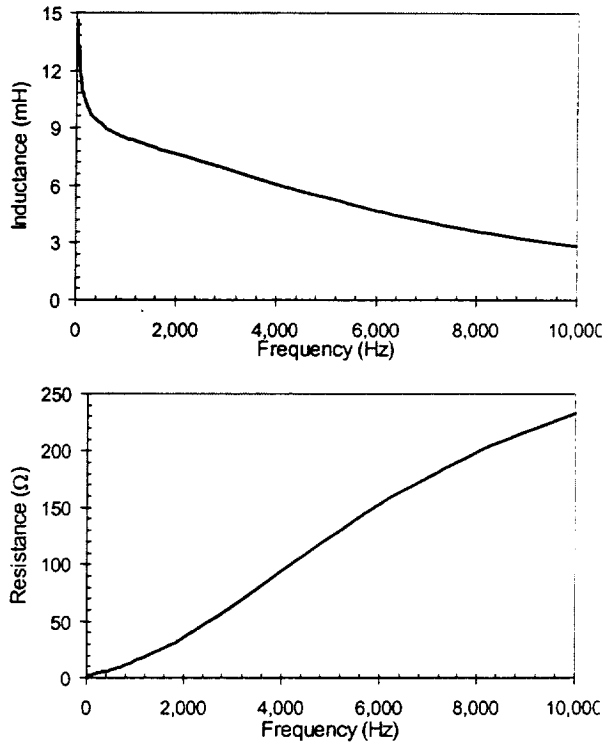


*Figure 10. Measured actuator impedance.*

### Positional Stiffness Measurement

Predicted versus measured positional stiffness is shown in figure 11. Measured stiffness is 70 lb/mil (123kN/cm), compared to 50 lb/mil (87.6kN/cm) predicted by FEA, assuming a 93% lamination packing factor (PF). As expected, this actuator exhibits highly linear positional stiffness.

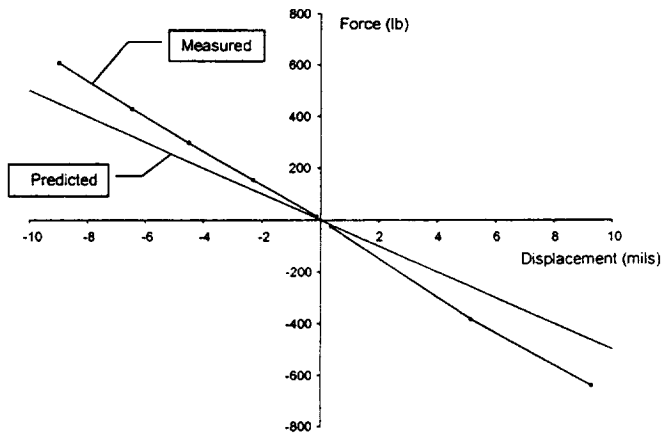


*Figure 11. Positional stiffness, predicted vs. measured.*

### Output Force Measurement

Output force as a function of DC and AC actuator current is plotted in figures 12 and 13. Figure 12 shows predicted and measured DC bearing performance; measurements show that actual DC forces are substantially greater than predicted. Bearing design and initial force predictions were done based on a lamination PF of 93% (the packing factor predicted by the lamination vendor). Also plotted is the predicted

in-line force vs. current for 98% PF. As demonstrated in the figure, the predicted force output for this bearing is highly sensitive to the assumed PF.

To reconcile the difference between predicted and measured forces, Hall sensors were used to map the bias flux density distribution in the bearing air gap (see figure 14 regarding bias field prediction and measurement). New FEA was then done to determine whether an adjustment in PF would produce reasonable agreement with the measured field distribution. At 98% PF, good agreement was found for both the bias field distribution and for in-line radial force (the diagonal force FEA predictions are not yet complete). Further study is required to determine the actual PF and establish whether some other factors are responsible for the predicted versus measured force disparity.

In figure 13, force vs. current is plotted for DC current at 50 Hz. As seen by comparing figures 12 and 13, the current stiffness (force per unit current) is significantly greater

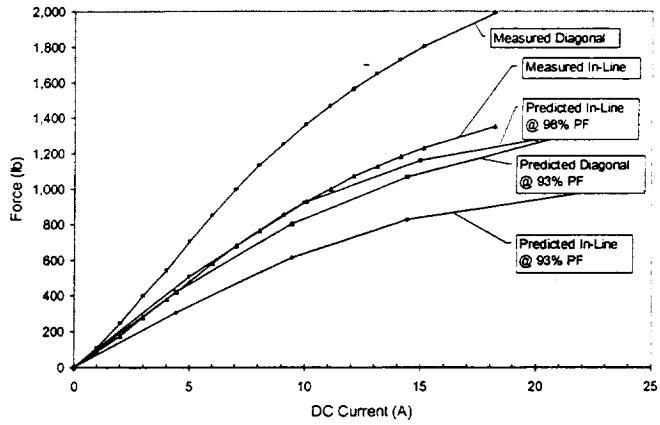


*Figure 12. Actuator force vs. DC current, predicted vs. measured.*

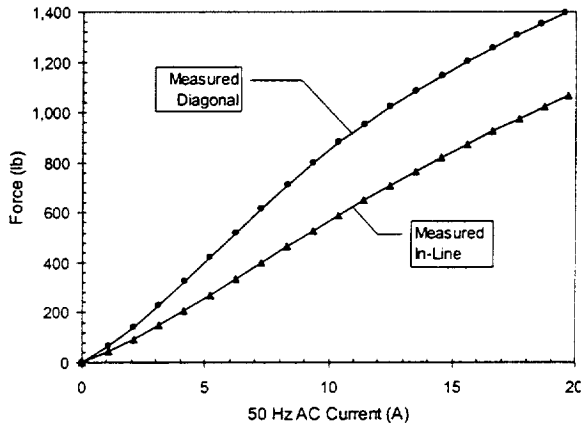


*Figure 13. Measured actuator force vs. AC current.*

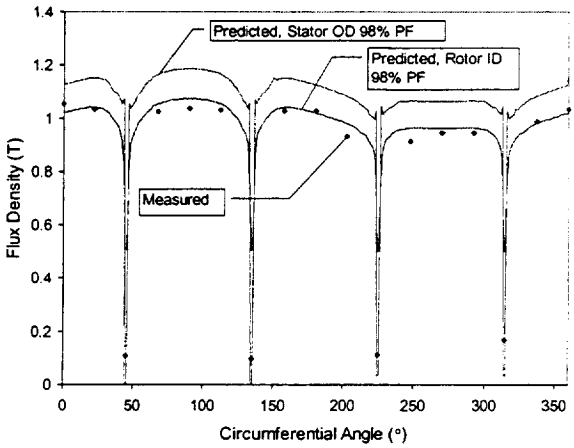


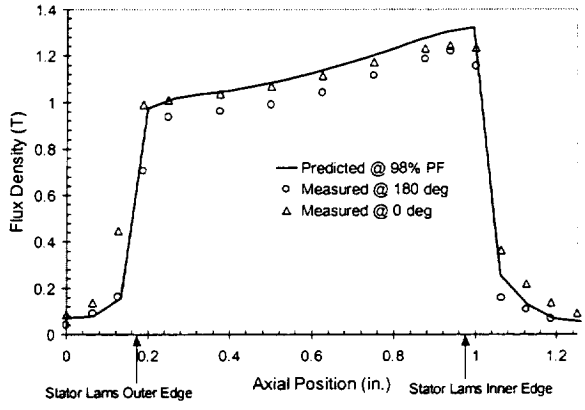


*Figure 14. Air gap flux density distribution, predicted vs. measured.*

for DC than for AC current input. This characteristic is confirmed in a transfer function plot presented later. Although AC current stiffness is less than at DC, the actuator still meets stated load capacity requirements, and exhibits nearly linear behavior.

## Air Gap Flux Density Measurement

Hall sensors were inserted into the bearing air gap to directly measure the bias flux density distribution. Predicted and measured field distributions as a function of circumferential angle and axial length are plotted in figure 14. The predicted field levels are plotted for a 98% lamination packing factor, which gives good agreement with experimental results.

## Transfer Function Measurement

Current stiffness magnitude and phase angle versus frequency are plotted in figure 15 for actuator currents of 1 and 5 A. Measurements were done for a maximum frequency of 200 Hz to avoid bearing fixture natural frequency modes above 200 Hz. Two transfer function plot characteristics are especially noteworthy: the current stiffness magnitude at DC is substantially greater than that measured above 50 Hz (also see figures 12 and 13), and a consistent 20° phase lag was measured between input current and output force. Knowledge of the phase lag is particularly valuable for accurate control system modeling. Magnetic hysteresis in the 4130 steel rotor lamination material may be responsible for the phase lag, and could be a consequence of choosing a structural steel for this component.

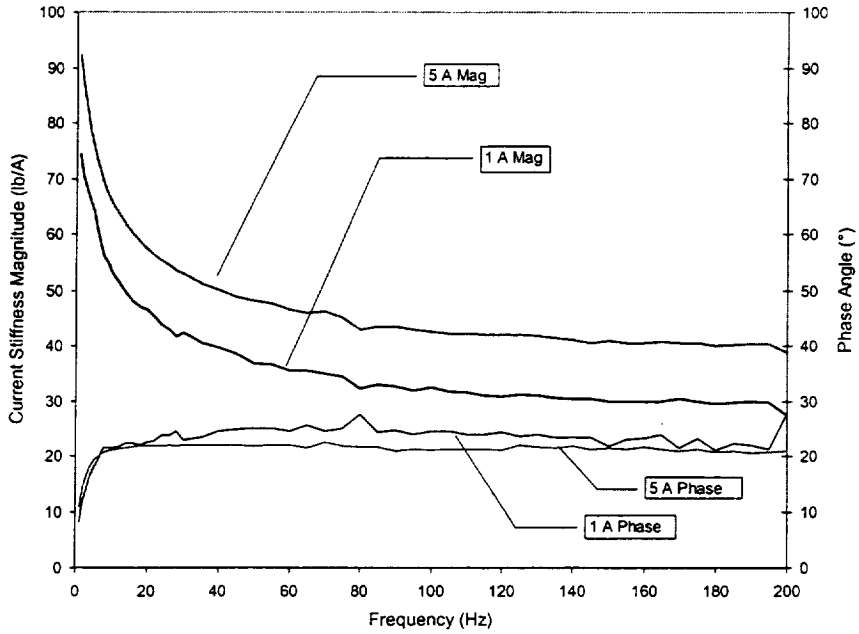


*Figure 15. Measured actuator transfer function.*

Magnetic Hysteresis Measurement

During bearing testing it was observed that the bearing force at zero current was not consistent, but appeared to depend on the current magnitude of the previous test. To test the hypothesis that this was hysteresis-induced behavior, a series of DC current pulses from zero to 18 A was input to the bearing, and the residual force recorded after each pulse was complete and current was re-zeroed. The resulting curve shown in figure 16 strongly suggests magnetic hysteresis behavior, and could explain the transfer function phase lag previously measured.

The most likely source of this behavior is the 4130 structural steel laminations; tests are currently underway to directly measure hysteresis characteristics for the 4130 and other materials used in the test bearing. If excessive, hysteresis would result in unacceptable bearing power losses and heating.

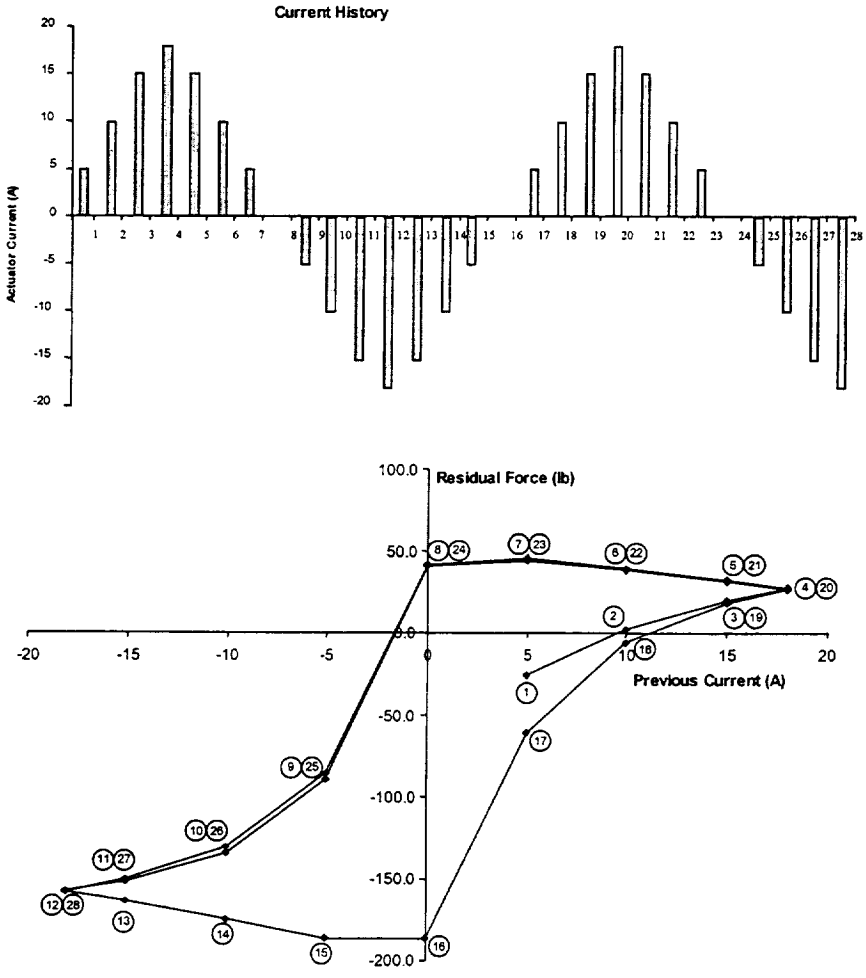


*Figure 16. Residual force measurement.*

## CONCLUSIONS

Researchers from UT-CEM have designed inside-out configuration active magnetic bearing actuators for use in a flywheel alternator for a hybrid-electric combat vehicle. This is the first known application of magnetic bearing actuators incorporating an inside-out topology. A prototype radial bearing was successfully fabricated, assembled, and tested in a bearing test fixture that directly measures important bearing parameters. Although measured bearing parameters meet performance goals, further work is underway to fully understand bearing behavior. Knowledge gained from this work will permit more accurate electromagnetic and control system modeling, and is an important step in the successful implementation of inside-out bearing actuators.

## ACKNOWLEDGEMENTS

The authors wish to thank Marilyn Freeman of DARPA for her support of this work. In addition, we want to acknowledge the contributions made by UT-CEM technicians Robert Arndt and Richard Rodriguez to the successful completion of this project. Finally, we wish to thank Vicki Heydron and Roy Pena for their assistance in the publication of this paper.

## REFERENCES

1. G. Buckner, A. Palazzolo, J. Kajs, B. Murphy, and J. Beno, "Control System for Inside-Out Configuration Magnetic Bearings," 5th International Symposium on Magnetic Suspension Technology, Dec 1-3, 1999.
2. M. Kasarda, P. Allaire, P. Norris, C. Mastrangelo, and E. Maslen, "Experimentally Determined Rotor Power Losses in Homopolar and Heteropolar Magnetic Bearings," International Gas Turbine & Aeroengine Congress & Exhibition, Stockholm, Sweden, June 2-5, 1998, ASME Publication No.98-GT-317.
3. G. Schweitzer, H. Bleuler, and A. Traxler, *Active Magnetic Bearings: Basics, Properties, and Applications of Active Magnetic Bearings*, vdf Hochschulverlag AG an der ETH Zurich, 1994.